Egyptian Journal of Chemistry

http://ejchem.journals.ekb.eg/

Magnetic Graphene nanocomposite: Synthesis, Properties, and Biological Applications

Ahmed M. Bakr

Spectroscopy Department, Physics Research Institute, National Research Centre, 33 El Bohouth St. Dokki, P.O. 12622, Giza, Egypt

Abstract

Graphene research has become an emerging frontier in materials science due to its exceptional electrical and thermal conductivity, high mechanical features, electron mobility, and its high specific surface area. Excellent characteristics of graphene deliver it to developed and applied in various applications. A combination of iron oxides nanoparticles (IONPs) and graphene produces a magnetic graphene nanocomposite. The received structure not only has the characteristics features of magnetization and a large specific surface area, but also it can improve the other remarkable disadvantages in the singular nanomaterials as the aggregation of IONPs and the low recovery of the graphene from the dispersion solvent. The magnetic graphene nanocomposite can be fabricated through various designs techniques such as natural blending of graphene derivative and magnetic nanoparticles, in-situ synthesis of the magnetic nanomaterials on graphene derivative, and covalent functionalization. The magnetic graphene nanocomposite can be potentially used in several biological and environmental applications such as MRI, drug delivery systems, hyperthermia, combined therapy, immobilization, and the adsorption of heavy metal, radioactive metal ions, and pesticides. In this article, the preparation procedures, properties, structure characteristic features, biocompatibility, and the biological-environmental applications, will be highlighted. Furthermore, challenges, visions, and prospects on the future trends have been introduced as concluding comments.

Keywords: Magnetic Graphene, Characteristic features, Synthesis approach, biological application.

1. Introduction

Ideal graphene is the first discovered and fabricated 2D crystal of one atomic layer thick arranged in a honeycombed like structure network with six-membered rings. Graphene has excellent potential in biological applications and graphene-based composites have shown promise due to their novel structure and physicochemical features. These meaningful outcomes are a primary result of the exhaustive consideration that such nanocomposites have brought up in the last years, as proved from the number of publications [1][2][3][4][5].The term graphene is firstly recommended by Boehm et al, in 1986 as a single carbon layer. Graphene name is formed of the prefix (graph) points to graphite, while the addition (ene) refers to the double bond C–C [6][7].

Lately, expression of graphene was formalized by IUPAC (the International Union for Pure and applied Chemistry) [8][9]. Devotedly, During the last 5 decades, intense attempts have been carried out to manufacturing an isolating a single layers of graphene [10]. Nevertheless, in 2004, a single atomic layer from graphite was isolated by Geim and co-workers, which led to comprehensive study on graphene [11]. Actually, Graphene can be described as a semi-metal or a semiconductor by zero bandgaps with high opacity and a low absorption degree of white light [12]. Furthermore, Graphene has high electron mobility (250,000 $cm^2V^{-1}s^{-1}$) [13], a high surface area (2630 m^2g^{-1}) [14], large modulus of elasticity (nearby 1 TPa) [15], great mechanical strength, and chemical stability [16]. Graphene oxide GO, reduced graphene oxide rGO, and graphene

*Corresponding author e-mail: ahmedbakr_8@yahoo.com.; (A. M. Bakr).
Receive Date: 30 December 2021, **Revise Date:** 12 January 2022, **Accept Date:** 16 January 2022
DOI: 10.21608/EJCHEM.2022.113755.5167

quantum dots GQD, are example of the graphene species [17]. Recently, Magnetic nanocomposites (MNCPs) have explored huge attention of researchers because of their magnetic natural features, large specific surface area, and high adsorption capacity, which support their enhanced approachability to active sites and improved its usage in interesting applications [18][19][20][21]. Moreover, the magnetic nanoparticles may be manufactured from hard to soft magnetic materials [22]. Generally, Iron oxide nanoparticles IONPs are a group of the magnetic matters which have been employed in various applications. If the sizes of the IONPs are less than a single magnetic domain, they can behave as superparamagnetic. (SPIONs) possess attractive features such as powerful magnetic saturation, and big field irreversibility, and as the outside field is eliminated, the SPIONs no longer display magnetic interactions [23]. Latterly, developed investigations with several varieties of iron oxide nanoparticles (IONPs) have been achieved, involving Fe_3O_4, α-Fe_2O_3, γ-Fe_2O_3, ε-Fe_2O_3, β-Fe_2O_3, and FeO [24]. Between these species of iron oxides, γ-Fe_2O_3 and Fe_3O_4 nanoparticles view the various favorable current candidates to employment in biological applications due to their outstanding biocompatibility, excellent chemical stability, and no distinct actual toxicity [25][26]. Aside from this, IO itself can be naturally presented in the human body and degraded over metabolic pathways [27]. The interplay among IONPs and the external magnetic field, and interplays between nanoparticles, would generate energy changes within the system and could deposit solid support for the employment of IONPs in biomedical science [28].

The incorporation of IONPs and graphene provides magnetic graphene nanocomposite (MG), which has not only the characteristics features of superparamagnetic and large specific surface area but also enhance disadvantage for the singular nanomaterials (the weak restoration of the graphene from the dispersion solvent, the agglomeration of IONPs,). The graphene derivatives can gain magnetic properties with the aid of SPIONs of magnetite (Fe_3O_4) and maghemite (γ-Fe_2O_3), and large binding site activity, high chemical stability, size coordination, simple modification, and good biocompatibility [29]. Several approaches were reported for the fabrication of IONPs, graphene, and MG [30][31]. Generally, the employment of different synthesis approaches have an impact on the obtained product features [32], and the biological applications can be influenced by the synthesis of the nanomaterials being used. Lately, MG has been employed widely in numerous applications as drug delivery [33], bio-imaging [34], extraction and chemical separation [35], MRI, and photodynamic and magnetothermal therapy of tumors [36]. Briefly, the preparation procedures, structure characteristic features, and biocompatibility of G and MG, will be highlighted. Moreover, we outlined the study of biological and environmental applications of MGO in the respect of MRI, drug delivery systems, hyperthermia, combined therapy, immobilization, and the adsorption of heavy metal, radioactive metal ions, and pesticides. In addition, challenges, visions, and prospects on the future trends have been introduced as concluding comments.

2. Properties and characteristic features of Magnetic Graphene (MG)

2.1. Graphene properties

Graphene composed of a two-dimensional layer with a single atom thick planar sheet of sp^2-bonded carbon atoms pound in a honeycomb lattice crystal [12][37]. When graphene sheets are stacked, it produces the three-dimensional formation of graphite with an inter-planar spacing of 0.34 nm, as shown in fig (1). Carbon sp^2 packed atoms have a molecule bond length of 0.142 nm [38].

Graphene has high mechanical properties with tensile strength nearby 125 GPa and elastic modulus of 1.1 TPa, which presents the strength of graphene to be 100 times stronger than steel [39].

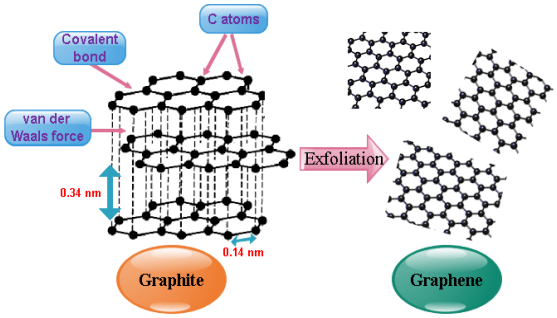

Fig. 1. Structure of Graphite (multi layers) and Graphene monolayer

Graphene is a good conductor, Graphene has extremely electrical features with a high carrier rate of about 15,000 cm^2/V.s, and outstanding high electronic mobility up to 2.105 cm^2/V.s, comparably, higher than 100 times of silicon. The thermal conductivity of graphene is about (5000 Wm^{-1} K^{-1}), henceforth 10 times higher than that of copper

(401 Wm^{-1} K^{-1})[40]. Among the most outstanding properties, graphene shows a very low density with a large surface-specific theoretical area (2630 m^2 g^{-1}), and an optical transmittance of about 97.7 % [41]. Graphene is an extremely conductive material, with a structure composed of sp^2 hybridized carbons, as shown in (Fig. 2) [42][43]. Each carbon atom in the lattice is packed with 3 σ bonds, which are connected to other atoms in the structure and 2 π bonds that are perpendicular to the σ bonds. For free-standing graphene layer, π bonds behave as free π electrons and move freely in the structure as they are not attached to any other carbon and , which stays mobile and can be delocalized through the graphene sheet. So, graphene is a good conductor with a high carrier rate of 15,000 cm^2 /V.s at room temperature [44].

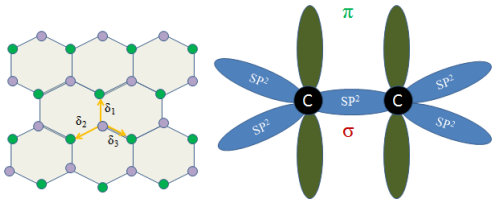

Fig. 2. sp^2 hybridized graphene

The bandgap is the minimum energy needed to excite the electron of valence to the conduction band. During metals conduction, the valence and conduction bands are connected, so the metals have no or zero bandgap, implying there is no energy used for conduction. Also, Graphene has no bandgap and it is frequently named a zero-gap semiconductor or zero-gap metal [45]. Within graphene hexagonal lattice structure, the Valence and conduction bands take the cone shape and connect at 6 spots called Dirac points, symbolizing the 6 vertices of the hexagonal lattice, as it presented in Fig. 3. The cones meet each other at K point (K and K') and are presented in the Brillouin zone which they stated the Dirac points of A and B carbons, r is the center of the hexagonal shape, b_1 and b_2 are reciprocal lattice vectors, kx and ky are 2D wavevector components along with the x and y directions, and M is the saddle point [46][47]**.** The valence and conduction bands contact in K and K' at the Fermi level means energy 0 Ev. Additionally, the masses of electrons and holes are almost near zero at this point, and as the electrons in graphene have zero mass, they move like a zero mass particle and give travel faster than any other conductor at room temperature [48].

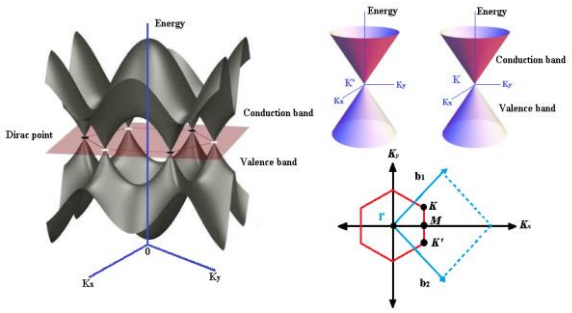

Fig. 3. The bandgap structure of graphene.

Indeed, the numerous distinguished graphene derivative is the oxidized shape referred to as "graphene oxide" (GO). Go has in its formation numerous oxygen-containing functional groups, i.e. epoxy, hydroxyl, carbonyl and carboxylic (--COOH) groups [14]. The plenty of the oxygen functional groups gives the GO its hydrophilicity and responsible for dispersions stability of GO nanosheets. In addition, GO is negatively charged and acts as a polyanion, and can combine electrostatically with positively charged materials [49]. Furthermore, GO has superior adaptability with polymers and metals, and therefore it can be applied in the generation or functionalization of membranes combined with positively charged materials. That substance, which can be achieved by graphite exfoliation with chemical oxidation, was highlighted lately due to its benefits for many application possibilities. GO can be obtained in large amount from graphite, and its fabrication costs are decreased in association with different graphene and carbon-based materials, which improves the chance of its employment in a wide variety of applications [50].

2.2. Characterization of Magnetic Graphene (MG)

The characterization of MG reveals the chemical and physical characteristics features of the manufactured materials, thereby recognition of which particular features/characteristics of special application can be performed. MG can be recognized based on the magnetic features, morphology, surface area, chemical structure, and thermal properties. The characteristic features can be identified by several experimental techniques such as Fourier transform infrared spectroscopy (FT-IR), Raman spectroscopy, X-ray diffraction (XRD), Transsmetion electron microscopy (TEM), scanning electron microscopy (SEM), and vibrating sample magnetometry (VSM).

(FT-IR) spectroscopy can be applied to distinguish the chemical structures of MG through determining its adsorption peak and whichever is assigned to. For GO, the stretching vibration associated with hydroxyl group can be recognized at 3240 cm^{-1}. The band located at 500, 506, and 514 cm^{-1} are exhibiting the interaction that occurred between Fe-O. C=C aromatic stretching vibration is presented at about 1680, and 1689 cm^{-1} for the MGO, while the band presented at 1411, 1471, and 1491 cm^{-1} is attributed to the ring C-C bond. C=C-H stretching vibration can be assigned to the band at 930, 934, and 944 cm^{-1} [51][52][53][54][55]. The magnetic properties of MGO can be measured using (VSM). The magnetic saturation higher order, compared to the value of bulk iron oxide, reveals the effectiveness of the prepared IONPs and can be affected by the appearance of added nanomaterial(s) to the surface of the IONPs. The investigation of the MG structure and their surface morphology can be shown by TEM and SEM. GO is seen as an irregular shape sheet with wrinkled, and the SPIOs are recognized as small spherical nanoparticles decorated and scattered diffused on the surface of the GO sheet [56][57]. Basically, The XRD investigation is employed for the identification of the crystalline formation of MG. Through examining the prepared sample within a range of 2θ angles, while each of potential diffraction of the lattice could be attained attributed to the irregular orientation of the samples. XRD spectra of graphite and GO revealed diffraction peaks attributed to the (002) plane for graphite and shift to (001) diffraction plane. MGO displays distinguished characteristic peaks attributed to the cubic phase structure of Fe_3O_4 in MGO composites (220), (311), (400), (422), (511) and (440) located at 2θ = 30.1, 35.5, 43.1, 53.4, 57.0, and 62.67 [56][58]. Furthermore, Raman spectroscopy is an essential technique for the qualitative characterization of MGO nanoparticles. The characteristic Raman spectrum of GO is identified by G band at 1605 cm^{-1}, which is associated with the E_{2g} phonon of the sp^2 C atoms (in-plane vibration of sp^2 carbon atoms in a 2D hexagonal lattice), while D band at 1353 cm^{-1}, which assigned to the breathing mode of *k*- point phonons of A_{1g} symmetry (vibrations of sp3 carbon atoms). The G band belonging to graphene was noted at 1600 cm^{-1}, which is slightly shifted from the position of that of GO. The D band is an indication of disorder, attributed to particular deficiencies as vacancies, grain boundaries, and amorphous carbon species [59][60]. The ratio of the peak intensity relative to the D to G band (ID/IG) is valuable information used to assess the ordered and disordered crystal structures of carbon and quality of the obtained materials. ID/IG slightly decreased in the case of graphene from the ratio of GO. This difference indicates the repair of defects by recovery of the aromatic structures. Two other bands were observed at 2700 and 2900 cm^{-1}. The band at 2700 cm^{-1} is known as the 2D band, which is an indicator of the number of graphene layer. The broadened in this band mainly attributed to the graphene contains few layers with some defects. Another band, known as the S3 band (2900 cm^{-1}), is a second-order peak derived from the D–G peak combination. The intensities of both peaks increased in the case of graphene compared to those of GO [61][62].

3. Growth mechanism of Magnetic Graphene (MG)

3.1. Graphene Synthesis

Since its discovery in 2004, many invention methods of graphene have been announced. Ordinarily, top-down and bottom-up are the two kinds of approaches to fabricate graphene, as pointed in (Fig. 4), and more extra discussion about the main methods is revealed below [63][64][65][66][67][68][69].

3.1.1. Top-Down Methods

Actually, graphene can be obtained by exfoliation of graphite, which is commonly utilized as beginning substance. Mechanical exfoliation, chemical/ electrochemical peeling, and chemical/electrochemical synthesis are the principal techniques in the top-down procedure. The top-down fabrication techniques are very simple to achieve graphene mass production [63][65]. The main top-down techniques, which are regularly employed by scientists to fabricate graphene, are stated below:

- ***Exfoliation method***

Mechanical peeling, chemical exfoliation, and electrochemical exfoliation are the main types of exfoliation, which considers simple and popular methods for graphene fabrication from graphite. The primary method used to get one layer of graphene applying mechanical exfoliation of graphite was developed by Novoselov and Geim and is quite popular as the Scotch tape technique [70][71]. By

2010 they won Nobel Prize in Physics due to their achieved results by performing this technique. A chemical peeling is a powerful technique to produce massive quantities of graphene. Nevertheless, that technique has some drawbacks, such as it involves complicated chemical processes as it more usually provides sheet-shaped of graphene with low conductivity [72]. Liquid phase exfoliation (LPE) is an innovative top-down method that simply involves exfoliating ordinary graphite by high-shear mixing or sonication [73]. Yet, two various graphite peeling methods are utilizing LPE, and those are cavitation in sonication and high-shear mixing. Practically, the LPE operating conditions are very easy and do not require a vacuum or high-temperature operation [74].

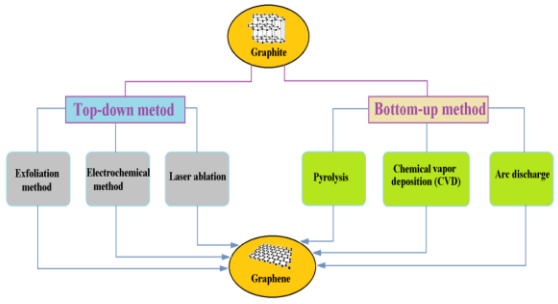

Fig. 4. Growth mechanism of Graphene

- ***Electrochemical method***

Graphite exfoliation generated with electrochemical techniques has become a simple, meanwhile high-yielding process in recent times for the mass production of graphene. The anode, cathode, electrolyte, and power supply are the four principal components employed in the electrochemical technique. The graphene can be occupied by oxidizing and exfoliation of the anode, which is formed of a carbon source, meanwhile, the cathode can be changed by utilizing either platinum or graphite [11]. Wang et al. in their research utilized a graphite source as electrodes also employed a solution of PSS (Polysodium-4-styrenesulfonate) dissolved in deionized water as an electrolyte, with an applied constant current of 5 V. Dray powdered graphene was obtained after 4 h of the exfoliation process by isolating it from the cell, followed by washing the dispersion powder with deionized water than alcohol, finally, vacuum drying. The achieved dispersion powder has been found to be extremely stable [75]. Parvez et al. employed graphite source as the anode while using platinum (Pt) as the cathode.156 the electrolyte solution containing sulfuric acid, and the two electrodes were soaked in it for 10 min under a potential of +10 V. The yielding graphene powder of this process formed about 60% with a few layers (1–3 layers). They stated that sulfuric acid could be used as a suitable electrolyte during the electrochemical intercalation and exfoliation graphite process [76].

- ***Laser ablation***

Laser ablation becomes a new synthesis method to fabricate numerous nanomaterials, particularly graphene. This technique has encouraging advantages, as it is environmentally friendly with simple experimental settings (no need of strict conditions), long-lasting graphene stability with a free unwelcomed contaminant in graphene outcomes furthermore avoiding the employed of dangerous reactants during the process [77]. Cappeli et al. employed laser ablation in graphene fabrication. In their study, they used substrates of silicon (Si) with changes in applied temperature (of room temperature up to about 900 °C) applying laser Nd:YAG laser operating in the near IR (λ = 523 nm, repetition rate (v) = 10 Hz, pulse width (τ) = 7 ns, fluence (ϕ) ≈ 7 J cm^{-2}, deposition time = 15 min).175 Then, the developing technique is achieved including a variety of conditions to receive the high-quality product of graphene [78]. Graphite can be used as a carbon source during Laser ablation techniques and erode the carbon surface to fabricate graphene by adjusting several parameters throughout the synthesis method of graphene according to the laser ablation operation which can influence the graphene quality. The controlled parameters in the laser itself like laser fluence, repetition rate, wavelength, also pulse duration should be adjusted during the synthesis process. Additionally, the choice of the substrate mainly affects the graphene product, besides the pressure and the gas background, temperature of the substrate, and the distance of substrate [79].

3.1.2. Bottom-Up Methods

The bottom-up strategy depends on the deposition of the starting element (carbon source), and graphene can be obtained by controlling variables and conditions like gas flow rate, pressure, and temperature. The bottom-up technique can yield a high-quality graphene product, besides good electronic features with some structural defects. Nevertheless, mass production is relatively small,

which can be employed for a limited field. Some of the bottom-up techniques that are regularly employed in graphene fabrication are listed below [63].

- ***Pyrolysis***

The word pyrolysis generated from the Greek-derived component *pyro* and *lysis, Pyro* stands for fire, and *lysis* means to detach. In this technique, a manufactured carbon atom at a metal surface is a simple method employed to manufacture graphene few-layer [80]. Silicon carbide (SiC) thermal decomposition is one of the popular procedures of graphene synthesis, as Si is desorbed at a high temperature giving behind C atom which creates graphene of few layers. This method has gained important development through the continuous graphene films generation on thin film of nickel-coated on SiC substrate at a high temperature of 750 °C [81]. A similar method is employed in thermal decomposition of ethylene at high temperature and characterized by the generation of high purity of graphene mono-layer, however, this approach suffers from low production and cannot be utilized in large scale of graphene synthesis [82].

- ***Chemical vapor deposition (CVD)***

Chemical vapor deposition (CVD) is one of the most popular bottom-up synthesis techniques and one of the most useful methods employed for the generation of high-quality graphene with a large-scale basis. This technique includes joining a gas molecule with a surface substrate in a reaction chamber under controlled conditions of temperature, pressure, and gas flow rate. The mechanism of CVD technique used in graphene synthesis mainly depends on the substrate employed and several types of substrates are utilized in CVD for graphene film growth, mainly involving Nickel (Ni), Copper (Cu), Iron (Fe), and Stainless steel [83][84]. Methane (CH4) and acetylene (C_2H_2) are usually employed as carbon sources. Choice of the substrate is a significant element in order for the graphene side to be able to be manufactured. While using Ni substrate, under high temperatures and employing carbon as a raw material to create graphene which dissolves in Ni and the dissolved carbon is separated and precipitated to get graphene throughout the suitable cooling rate. On the other hand, when Cu substrate is used in graphene synthesis during CVD process, carbon is deposits directly at the Cu surface substrate. Particularly, several parameters that affect the process of graphene synthesis in the CVD method include substrate quality, oxygen at the substrate surface, pressure, temperature, and the C/H ratio. The numerous interdependent parameters in this CVD technique ordinary influence the controlling method of the quality and the structure of the obtained graphene. Generally, there are two CVD methods mainly applied involve; thermal CVD and plasma-enhanced CVD (PECVD). Thermal CVD includes a high-temperature heating furnace, vacuum tube, vacuum pump, vacuum gauge to control pressure, and a mass flow controller to adjust carbon and career gas employed in graphene fabrication. While PECVD technique plasma drives the decomposition of the gas source and reacts with metal substrate leading to the creation of graphene film. Power sources as (DC) direct current, (RF) radio frequency, and microwave have been employed as a source of plasma. The advantage of plasma-enhanced CVD over thermal CVD is that the creation mechanism can happen with low temperatures and pressure[85].

- ***Arc discharge***

Comparatively, the arc discharge is an environmentally friendly approach for graphene fabrication with cost-effective value. Graphene is fabricated by the arc discharge process under a gas flow of helium (He), hydrogen (H_2), or nitrogen (N_2). Wu et al. (2010) reported that the arc discharge method can be developed to generate graphene with few-layered under the combination of He and carbon dioxide (CO_2) mixture [72]. The obtained result presents the received graphene has fewer drawbacks than that gained through chemical methods and is easily dispersed in organic solvents toward further applications. They revealed that the blend of He and CO_2 throughout the arc discharge method is able of creating graphene with good properties for manufacturing electrodes to various devices. Furthermore, the graphene generated by utilizing such a technique is performed as a suitable selection for an electric charger employed in conducting nanocomposites. Kim et al. in 2016 developed a scalable and controllable aqueous arc discharge method that can yield bi- and trilayers of graphene with high quality [86]. Nevertheless, they reported that a separation technique was required for the development of this method.

3.2. Graphene oxide (GO) Fabrication

The graphene family contains of graphene oxide GO, reduced graphene oxide rGO, and graphene

quantum dots GQD, among others. GO is the oxidized form of graphene as the oxygen functional groups on the GO presented, (epoxy, hydroxyl, carbonyl, and carboxylic groups), which give GO hydrophilicity. The GO contains aliphatic (sp^3) domains and aromatic (sp^2) which improves the variety of the surface interactions. Generally, there are three main methods to create GO can be applied, namely the Brodie's (Brodie, 1860), Staudenmaier's (Staudenmaier, 1898), and Hummer's (Hummers and Offeman, 1958) methods [87]. Each method is dependent on the chemical oxidation of graphite by strong acids. Originally, Brodie's method was the commonly used method, graphite was blended with fuming nitric acid and potassium chlorate, subsequently, and it became a highly time-consuming and unsafe process. Thereafter, nearly 40 years later, Staudenmaier developed that process by substituting components of the fuming nitric acid for concentrated sulfuric acid, and further the chlorate was added in batches [88].

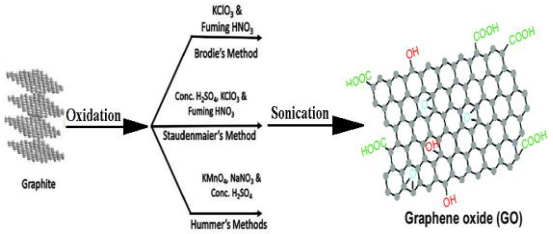

Fig.5. Graphene oxide production

By 1958, and depending on both these processes, Hummer's method was designed by Hummers and Offeman and is based on the original obtention of graphite oxide, through two oxidation procedures, and is commonly utilized for GO fabrication nowadays. During this process, the obtention of GO is provided by the peeling of the graphite oxide by using ultrasonic waves in aqueous media, then the graphite oxide three-dimensional form was splitted, and the brown-colored solution including individual nanosheets of GO can be provided [89]. rGO can be obtained via the reduction of the GO. The reduction of GO is classified into chemical and non-chemical processes. Chemical reduction of GO includes reducing agents such as hydrazine and sodium borohydrate. While the non-chemical reduction of GO involves hydrothermal, solvothermal, and electrochemical reduction, etc. [57].

3.3. Synthesis approaches of MG nanocomposites

Magnetic materials, especially iron oxides nanoparticles (IONPs) are managed and particularly materials that could be handled with an external magnetic field. Owing to their particular small size and unique superparamagnetic feature, magnetic nanocomposites have been developed based on the combination between IONPs and other nanomaterials. Synthesis of magnetic graphene nanocomposites MG provides improvements such as large surface area and high separation speed. MG is mainly synthesized through physical and chemical techniques (Fig. 6) [90][91][92][93].

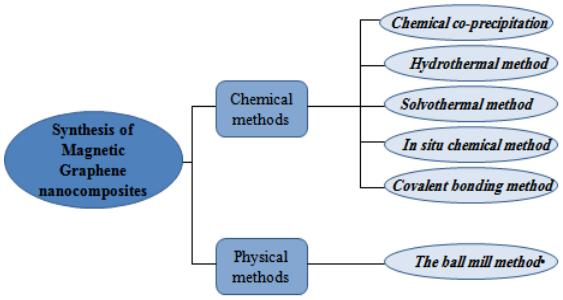

Fig. 6. Synthesis approaches of MG nanocomposites

- ***Chemical co-precipitation***

MG composites are synthesized in this method via the combination of a stoichiometric mixture of Fe^{3+} and Fe^{2+} to the graphene source suspension and the cationic and carboxyl interactions on the G or GO surface are created in the presence of inert gas. pH, temperature, and ionic strength of the precipitation medium are the main parameters that should be maintained in order to control the shape, size, and magnetization. Iida et al. stated that synthetic particles Fe_3O_4 created from iron chlorates had a higher saturation magnetization with a smaller particle size than that prepared by iron sulfates [94]. Hong et al. noted that, amongst the three distinct parameters in co-precipitation techniques, including the employment of $NH_3.H_2O$ in water, the utilize of NaOH, and the use of $NH_3.H_2O$ in alcohol suspension, the saturation magnetization of the IONPs Fe_3O_4 fabricated through co-precipitation with $NH_3.H_2O$ was higher than that of those prepared with NaOH. Coprecipitation with NaOH required the least time; however, coprecipitation with $NH_3.H_2O$ in water required the most time[95].

In general, the co-precipitation technique is manageable, mass production, non-toxic, economical, and controllable. While the manufactured composite have the drawbacks of the detachment of IONPs of

graphene nanoparticles and easy agglomerates of Fe_3O_4 and reduced graphene nanoparticles. Additionally, the employing of the alkaline precipitate solution, as KOH or NaOH, for preparing the precipitates and reduction of functional groups [96].

- ***Hydrothermal method***

The hydrothermal process starts with water as a solvent, then a specific portion of metal salt was added while the adjustment of pH using an alkaline solution, after that the blend is placed in a high temperature and pressure reactor for crystallization. Usually, the Hydrothermal method is green, scalable, effective, and economically, with the ability to reduce graphene oxide during IONPs synthesis. In addition, the chemical reaction takes place inside a high-pressure reactor of about 0.2-4 MPa, which can prevent the volatilization of components, and the high temperatures are another advantage to improving magnetism [56][97].

- ***Solvothermal method***

In the solvothermal technique, organic solvents can be used instead of water since a high boiling point reducing agent, and practically it is a development method of the hydrothermal process. The prepared composites have excellent dispersion in the polar medium with good stability. Furthermore, the IONPs properties, such as size, morphology, crystallinity, density, magnetism, and dispersibility, could be maintained by controlling the reaction parameters like the concentrations of the reactants, reaction time, properties of solvents, reaction temperature, and the ratio of reactants [90][98].

- ***In situ chemical method***

Several studies were developed to fabricate MG nanocomposites by in situ reductions of the iron acetylacetonate within a mixture of GO and triethylene glycol. The method is simple, and the graphene oxide does not require any modification. Through in situ chemical method by sodium citrate as the crystal growth inhibitor, ultrasmall IONPs could be effective with uniform joined to GO nanosheets. Chen et al. prepared MGO through an in situ growth process and revealed that PEGylated graphene oxide nanosheets were to be joined randomly by β-FeOOH. The method is cost-effective and the interactions between graphene and IONPs are effective, while, it is time-consuming [34][90][99],

- ***Covalent bonding method***

Frequently, covalent bonding techniques mainly modify the GO surface for the attachment of IONPs. Practically, the covalent joining between the magnetic nanoparticles and graphene oxide should require a functionalized well-established surface for both GO and magnetic particles, which was associated with the nanoparticle type. Fundamental sites of response by nucleophilic substitution could be the epoxy groups from GO sheets, which produce the bonding of groups with amino functionality (-NH2) possess lone pairs of electrons able to attack these epoxy groups. Generally, this is a comprehensive approach for the synthesis of well-controlled MG with cost-effectiveness, and the combination between GO and IONPs is powerful, however, it is time-consuming. He et al. mention the original tunable method to MG based on Fe_3O_4 and GO compound by a covalent method [100] [101].

- ***The ball mill method***

Usually, in this technique, both the graphene and magnetic nanoparticles are prepared separately, and MG nanocomposites can be obtained by mixing the graphene and magnetic nanoparticles. in this method, the magnetic nanoparticles can be physically bound to the nanosheets of graphene. But, the combination of this magnetic composite cannot withstand hard conditions as is not stable enough. Luo et al. fabricated $Fe_3O_4@SiO_2$ microspheres through solvothermal reduction, and (GO) by Hummers and Offeman processes. After washing the prepared GO and IONPs microspheres, water and N, N-dimethylformamide (DMF) were added to $Fe_3O_4@SiO_2$/GO dispersive solution and stirred vigorously. This technique ordinarily does not react at room temperature and can manufacture solid-gas chemical, solid-liquid, and solid-solid reactions. The ball mill method is simple and low-cost, as well as functional to large-scale production, but it is a complicated method and demands the controlling of several conditions to prepare the required structure, phase, and particle size. The magnetic characteristics of the nanocomposites could be maintained by controlling the composition applied and the milling time. In addition, the magnetic composites prepared via the ball-milled procedure could maintain the functional groups of GO [101][102].

4. Biological and environmental Applications

Actually, the magnetic graphene nanocomposites MG could be employed in a lot of environmental and biological applications due to exceptional physical and chemical features. The main features include the large specific surface area with suitable attach site activity, its magnetic and photothermal features, powerful chemical stability with plenty of chemical bonds, biocompatibility, and facile functionalization. In this section, several environmental and biological applications of MG will be reported

4.1. MRI contrast agents

Practically MRI contrast agents, according to the mechanisms relaxation of water protons, can be classed as T1 and T2, where MRI contrast agents T1 and T2 could magnify spin-lattice relaxation and improve the spin-spin relaxation of water protons respectively. Significantly, the magnetic iron oxides nanoparticles (IONPs) were examined broadly as T2 contrast agents [90]. In general, IONPs tend to aggregate and produce precipitation in real employing, which limits their purpose for in vitro and in vivo applications [105], therefore it is important to improve IONPs with fitting functionalities to manufacture the magnetic hybrids. Graphene derivatives as GO and rGO were efficiency utilized as a functionalized platform due to their large surface area, plenty of oxygenated functional group [103], biocompatibility [104], and can control the IONPs distribution symmetry within graphene sheets, accordingly holding the potential ability to utilized as MRI contrast agents.

Huang et al prepared MGO (MGO-COOH) and implied that the hydrophobic iron oxide nanoparticles cluster adhere to GO-COOH layers and compose water-dispersible order. They employed MGO as transferring agents and stated that GO could enhance the T2 contrast effects of the IONPs, which displayed a more excellent contrast enhancement in association with iron oxide only. Obviously, the signal-to-noise ratio (△ SNR) amount detected for MGO-COOH was higher in comparison with that recorded for the naked iron oxide, while SNR rate reduced with reaction time delay, moreover displaying that MGO-COOH could provide powerful signal loss in the tissue and cause higher contrast improvement [105]. The obtained results demonstrated that the employing of the MGO nanoparticles could raise the relaxation process, presenting useful use for the MRI negative contrast agent.

Furthermore, there used as T2 MRI contrast agents, MG revealed a powerful T1-weighted relaxation review as the diameters of the particles were decreased to a lesser 10 nm. Luo et al. investigated the performance of cis-aconitic acidedoxorubicin-SPIONs-GO (CAD/MGO) as T1-MR imaging and studied the in vivo MR imaging of the 4T1 tumor model. MRI signals of the tumor revealed notable development, with the tumor extent clearer after intravenous injection of (CAD/MGO), implying the fast improvement of CAD/MGO in the tumor area. Furthermore, and after 15 min, the MRI signals of the liver, kidney, muscle, and heart represented a slight increase; while, the MRI signals of the bladder revealed strengthened and arrived at the peak value at about 30min after injection. Clearly, the MR images of normal organs and the signal-to-noise tumor ratios (SNR) could be found, implying that the CAD/MGO composites could be utilized as powerful contrast agents for T1-weighted positive MRI of tumors in vivo [106].

4.2. Drug delivery systems

Amongst graphene derivatives, GO has been employed in different biomedical and biological applications including the usage as drug delivery systems, owing to huge specific surface area, excellent dissolvable in physiological solutions, high capacity of the functional groups, simple modification, and potential biocompatibility [101]. SPIONs of Fe3O4 nanoparticles is an example of the commonly employed magnetic materials used in the fabrication of MGO and could be applied to drug delivery application, which has the advantages of good biocompatibility with low toxicity, powerful superparamagnetism, near-infrared (NIR) absorbance, and a simple production process. The most chemotherapeutic factor used in malignancy therapy is Doxorubicin (DOX), with an active cell-killing ability, which limits its broad employing. So, the right transfer of DOX to the objective position is necessary to decrease its toxic effect on the human body and improve drug efficacy. Nanocomposites of drug delivery systems by managed deliverance for the medicine could possess moveable portals which can be locked and forced by inducements. The pH, light or AC magnet, and temperature could be used as drug delivery systems stimuli [101].

Liang et al. have bombined b-cyclodextrin-hyaluronic acid polymer (CDHA) with MGO to design a objective drug delivery multifunctional

(CDHA-MGO) [87]. The combination of MGO and polymer can efficiently enhance the release of (DOX), up to 485 mg/g. Additionally, the MGO, based on GO and Fe_3O_4, produced a simple photothermal response tool in order to control the DOX discharge which excited by near-infrared irradiation .

The cationic drug of Mitoxantrone (MTX) can be efficiently loaded via physical interactions with a negatively charged nano-combined. Jafarizad et al. noticed that MTX drug could be easily packed with an MGO-PEG-functionalized nanocombined via physical cooperations [107]. Pourjavadi et al. reported that the drug molecules of doxorubicin were laden and combined with MGO-polyamidoamine-nanocarrier by π-π stacking with graphene oxide nanosheets, moreover, covalently associated with a dendrimer via hydrazone connections, which dissociation of doxorubicin was pH-sensitive [90].

The acidic tumor surrounding considers an advantageous agent for drug loading and release of the drug-loaded on MG and powerful pH-dependent, which may be fundamentally associated with the weakening of the active hydrogen connection within GO and the drugs. The Combination of biological and magnetic targeting properties, within the drug delivery system could be primarily managed to collect at the locations of tumor cells by a magnetic field, then controlled the drug release via pH, light or AC magnet, and temperature. Additionally, several functionalizations could be employed to develop the drug release properties, biocompatibility, and durability of the MG within the physiological microenvironment. MGO conjugated-Pectin (PEC) (PEC-GO-Fe_3O_4) has been applied to develop a paclitaxel drug delivery system, and its association with the GO-Fe_3O_4 and PEC-GO-Fe_3O_4 take place by the support of hydrophobic link and π–π stacking among aromatic and hydrophobic groups from the paclitaxel and manufactured MGO nanocomposites. The medicine capture performance percents were 84.85 ± 5.3 and 78.3 ± 5.3 for PEC-GO-Fe_3O_4 and GO-Fe_3O_4, while the loading capacity percents were 36 ± 3.21 and 33.35 ± 3.10 for the prepared PEC-GO-Fe_3O_4 and GO-Fe_3O_4, respectively. The powerful performance and drug loading capacity are attributed to the changing of surface area by linked PEC and hydrogen bonding cooperations between the drug and PEC function groups [101].

4.3. Combined therapy

Chemotherapy involves applying cytotoxic anti-neoplastic drugs. Though, the therapy may decline due to the resistance toward the employed drug. The cancer cells begin to decrease the collection of the drug at its intracellular position. Accordingly, combined therapy can increase the treatment response and dominate drug resistance.

Xinxing et al. employed diagnosis and simulated combined therapy of PEG-functionalized GO- SPIONs hybrid nanocomposite loaded with (DOX). The manufactured system has a high absorbance in the visible to NIR range, which is advantageous for photothermal therapy targets with the magnetic field. The drug loading efficiency of the functionalized MGO reached 220%, and the drug discharge was 20% and 50% in the pH of 7.4 and 5.0, in 360 min, respectively. Besides, the functionalized MGO could be employed as the T2 contrast agent [108]. Lu reported the employment of MGO for combined therapy, which was prepared by adhesion Fe_3O_4 nanoparticles on GO sheets by the co-precipitation process and was applied for combined chemotherapy moreover photothermal therapy [109]. The prepared GO-Fe_3O_4 can be modified by PEG and Cetuximab (CET, an epidermal growth factor receptor (EGFR) monoclonal antibody) to get the magnetic hybrid (MGO-PEG-CET). The functionalized GO-Fe_3O_4 hybrid expressed DOX loading capacity of 6.4 mg/mg. The combined photothermal therapy represented by MGO-PEG-CET was applied as over its expression to near-infrared (NIR) and magnetically objective against CT-26 (colon carcinoma cell line). The comparable growth dimensions for the tumor-bearing BALB/C mice at day 14 were 12, 10, 9.5, 6, and 0.4 for the control (normal saline), the mice treated with DOX, GO-PEG-CET/DOX, GO-PEG-CET/DOX + magnet, GO-PEG-CET/DOX + magnet + laser. Consequently, the mice group, which was treated with combined chemo-photothermal therapy, comparison with the control mice, revealed a bout 30-fold improvement in healing ability [109].

Liang et al. synthesized rGO@Fe_3O_4 through spray drying and coprecipitation technique and employed it for combined chemo-photothermal therapy including magnetically objective. The NIR photothermal response of the prepared nanocomposite displayed high photothermal conversion performance, and the rGO@Fe_3O_4 has a powerful medicine loading capability of 18.34%. The drug release performance of the prepared MGO

nanocomposite is pH-sensitive and could be attributed to the partial protonation of the hydroxyl and amine groups of DOX resulting in increased drug dispersion and powerless of hydrogen bonds among the DOX and graphene. Hela cells treatment with rGO@Fe3O4/DOX until 4h with confocal laser scanning microscopy examinations revealed that there is observed intracellular fluorescence of DOX for the rGO@Fe_3O_4 with an magnetic field. Nevertheless, fluorescence weakening could be mentioned for the rGO@Fe_3O_4 without using a magnetic field, which means, the internalization of the prepared rGO@Fe_3O_4 is advanced by an applied magnet which reveals the efficacy of the synthesized nanocomposites to be magnetically manipulated [110].

4.4. Hyperthermia

MG nanoparticles can be employed as a magnetic hyperthermia agent at a localized cancer therapy. Cancer cells is more sensitive and facilely affected by moderate warm (~42°C) than normal cells owing to disorderly blood vessels, that decreased the blood supply around cancer region and reduced heat distribution to encirclement regions. The MG can be injected into the tumor position and magnetic field is applied to warm the tumor position resulting in their death. In addition, hyperthermia can be employed as a drug delivery excite agent and its combination with chemotherapy is a progressing cancer therapies [90]. Rodrigues et al. fabricated biocompatible water-soluble MG functionalized with copolymer pluronic F-127 and reported that the functionalized MG has a powerful packing capability reached 91% (w/w, expressing 910 μg/mg) of DOX with large heat response against display to the (AC) magnetic field. After 30 min, the drug delivery system can deliver about 46% of the loaded drug, while the drug released is only about 7%. In addition, the heating can happen by simultaneous magnetic heating, and also the heating can be produced by the NIR absorption [111].

4.5. Immobilization

Yan et al. fabricated a new model of MGO modified-amino acid nanocomposite used for the magnetic isolate of proteins. The MGO produced outstanding immobilization capacity toward bovine hemoglobin reached (868.3 mg g^{-1}) [57]. Nanocomposites MGO modified Polyvinyl alcohol owned efficiently immobilize proteases [112]. The obtained results revealed that the surface area reached 388.9 m^2/g, and the average diameter of the GO/Fe_3O_4/PVA nanocomposite was 9.6 nm, and the increase in the specific surface area means that the three-dimensional structure avoids the aggregate of GO sheets. This 3D structure produced a highest immobilization performance up to 91% for the porcine pancreatic lipase (PPL) enzyme.

4.6. Absorption of heavy metal

GO has plenty of oxygen functional groups, and can be effective separated with high absorption capacity. Accordingly, GO has the potential to be employed in the elimination of heavy metal ions. Because of the difficult isolation of the GO, MGO have been applied as adsorbate. MGO is a unique absorbent that simply could be isolated from aqueous medium, and is associated with high specific surface area, high chemical stability, easy functionalization, and magnetic separation capability and considers an ideal adsorbent for the removal of heavy metal ions from wastewaters [101].

MGO was employed for the removal of heavy metal ions in different pH and It was noted that the adsorption capacities for Ni^{+2} at pH 8, Zn^{+2} at pH 7, Cu^{+2} at pH 6, Cr^{+2} at pH 6, and for Pb^{+2} at pH 5.0 were 51, 63.7, 62.9, 24.3, and 200 mg/g, respectively [113]. In a different research, MGO was modified with polyvinylpyrrolidone and applied for the selective adsorption of the lead ions. The adsorption capacity reached 794 mg/g, and the remove percent of 99.8% of Pb^{+2} in a wastewater includes different metal ions. The mechanism of adsorption for the lead ions is chemical absorption, and the PVP group and electrostatic cooperation among Pb(II) and –COOH of Fe_3O_4/GO [114]. 3D Fe_3O_4/graphene foam with the provider of nickel has been utilized for the removal of Cr(IV). The 3D MG foam presented a high saturation magnetization, a high surface area, and displayed an absorption capacity of 259 mg/g for Cr(IV) ions, and quickly presented through the first 5 min, and reached equilibrium within 20 min. This active absorption is associated with the highly porous construction of the 3D foam with a high surface area which is helpful for the distribution of metal ions to the active sites [115].

4.7. Removal of dyes and pigments

MGO has been used for the removal of methyl violet and acid red 88 under various parameters. The obtained results displayed that, the adsorption

capacity was about 240 mg/g for methyl violet and 300 mg/g for acid red 88, while the adsorption is produced depending on the Langmuir isotherm. So, the MGO is a promising adsorbent candidate for the eliminate anionic and cationic dyes [116]. Chitosan modified MGO nanocomposite beads was employed for the adsorption of RB19 (blue 19) and Ni^{+2}. The hydrogen bonds between GO with oxygen-containing groups on its surface and the amine groups of the chitosan mainly enhanced the mechanical stability of the beads. The adsorption capacities of RB19 (blue 19) and Ni^{+2} were 102 mg/g and 80 mg/g [117].

4.8. Removal of radioactive metal ions

Wu et al. prepared MGO nanoribbons through a hydrothermal approach and applied them for thorium adsorption. They mentioned that the removing process of thorium using MGO is spontaneous and endothermic. Also, the removal of Th(IV) is affected by pH, adsorbent dosage, contact time, temperature, and initial concentration [101]. Zong et al. reported the synthesis of MGO modified by carboxymethyl cellulose and employed in the U(VI) removal. They showed that the absorption capacity of the modified MGO at pH 5.5 and 301 K reached 8×10^{-4} $mol.g^{-1}$. Zhongran et al. stated the preparation of MGO supported by polyamidoxime-polyethyleneimine and employed in the adsorption of U(VI). The modified MGO had a powerful adsorption capacity reached 600 mg/g at 298 K and pH 6.0. The U(VI) remaining concentration after elimination by the manufactured MGO in wastewater is lower than 6.4 μg/L and less than the allowable 30 μg/L for drink water. Accordingly, the manufactured modified-MGO is an encouraging absorbate for the elimination of radioactive ions from wastewaters [118].

4.9. Removal of pesticides

Rashidi et al. mentioned the synthesis process of MGO composed of GO-Fe_3O_4 nanoparticles supported by N-methyl-D-glucamine and employed to extract pesticides (chlorpyrifos and hexaconazole). The adsorption capacities for hexaconazole and chlorpyrifos reached 93.5 mg/g and 78.7 mg/g. The high absorption capacity for the manufactured MGO is associated with demonstration of adequate interactive forces of H-bonding between pesticides and the prepared MGO [119].

Fakhri et al. reviewed the preparation process of amine-functionalized Fe_3O_4-GO, which applied for MIL-101(Fe) supporting (MIL assigns to Material of Institute Lavoisier, while Fe-based MILs are photocatalysis agents). The prepared MGO nanocomposite was employed in the photo-degradation of both atrazine and diazinon. The degradation efficiency was 81 and 100 ± 1% for both atrazine and diazinon through visible light irradiation [120].

Conclusion and Challenges Prospective

In the presented survey, a brief history, the composition, characteristics features, preparation tools, and biological applications of the magnetic graphene nanocomposites are reviewed. The magnetic graphene nanocomposites have unique features as high specific surface area, massive absorption properties, promote water solubility, good biocompatibility, and magnetic properties that provide excellent applicable in biological applications. Various fabrication techniques of MG and their applications in several areas such as drug delivery systems, MRI contrast agents, hyperthermia, combined therapy, immobilization, removal of heavy metal ions, dyes, radioactive, and pesticides, were addressed.

Notwithstanding, the distinguished researches of MG and their usages in applications as photocatalytic, there is not sufficient study on these applications and require further investigation. MG can promote photocatalytic performance and enhance absorption features of other materials. Further enhanced magnetic graphene nanocomposites like magnetic graphene foams, graphene ribbon, and magnetic graphene quantum dots should be able to lead the management of future study purposes, in addition, their employing in different biological and environmental fields require to be examined. MG show some disadvantages as the agglomeration and detachment of the magnetic nanoparticles from the graphene structure require developed modifications and improvements in the fabrication techniques. Moreover, to investigate the broad potential of graphene economically, remarkable significant spots as long-term stability, toxicity and environmental influences require to be considered.

References

1. Ł. Dybowska-Sarapuk, A. Kotela, J. Krzemiński, M. Wróblewska, H. Marchel, M. Romaniec, P. Łęgosz, and M. Jakubowska, J. AOAC Int. **100**, 900 (2017).

2. A. N. Banerjee, Interface Focus **8**, (2018).
3. T. P. Dasari Shareena, D. McShan, A. K. Dasmahapatra, and P. B. Tchounwou, Nano-Micro Lett. **10**, 1 (2018).
4. M. A. Moharram, K. M. T. Ereiba, W. El Hotaby, and A. M. Bakr, Res. J. Pharm. Biol. Chem. Sci. **6**, 1473 (2015).
5. M. A. K. Moharram, K. Tohami, W. M. El Hotaby, and A. M. Bakr, React. Funct. Polym. **101**, 9 (2016).
6. N. A. A. Ghany, S. A. Elsherif, and H. T. Handal, Surfaces and Interfaces **9**, 93 (2017).
7. A. Bianco, H. M. Cheng, T. Enoki, Y. Gogotsi, R. H. Hurt, N. Koratkar, T. Kyotani, M. Monthioux, C. R. Park, J. M. D. Tascon, and J. Zhang, Carbon N. Y. **65**, 1 (2013).
8. H. A. Essawy and H. S. Ibrahim, React. Funct. Polym. (2004).
9. F. G. Torres, O. P. Troncoso, L. Rodriguez, and G. E. De-la-Torre, Sustain. Mater. Technol. **29**, e00310 (2021).
10. R. Mas-Ballesté, C. Gómez-Navarro, J. Gómez-Herrero, and F. Zamora, Nanoscale **3**, (2011).
11. B. L. Dasari, J. M. Nouri, D. Brabazon, and S. Naher, Energy **140**, 766 (2017).
12. W. Choi, I. Lahiri, R. Seelaboyina, and Y. S. Kang, Crit. Rev. Solid State Mater. Sci. **35**, 52 (2010).
13. A. K. Geim and K. S. Novoselov, Nat. Mater. **6**, 183 (2007).
14. Y. Zhu, S. Murali, W. Cai, X. Li, J. W. Suk, J. R. Potts, and R. S. Ruoff, Adv. Mater. **22**, 3906 (2010).
15. C. Lee, X. Wei, J. W. Kysar, and J. Hone, Science (80-.). **321**, 385 (2008).
16. F. Bonaccorso, A. Lombardo, T. Hasan, Z. Sun, L. Colombo, and A. C. Ferrari, Mater. Today **15**, 564 (2012).
17. S. Gurunathan, M. Jeyaraj, M. H. Kang, and J. H. Kim, Polymers (Basel). **11**, (2019).
18. L. P. Lingamdinne, J. R. Koduru, and R. R. Karri, J. Environ. Manage. **231**, 622 (2019).
19. A. M. El Nahrawy, A. B. A. Hammad, A. M. Bakr, B. A. Hemdan, and A. R. Wassel, Heliyon **5**, e02501 (2019).
20. A. B. Abou Hammad, A. M. Bakr, M. S. Abdel-Aziz, and A. M. El Nahrawy, J. Mater. Sci. Mater. Electron. **31**, 7850 (1234).
21. A. M. El Nahrawy, A. M. Bakr, B. A. Hemdan, and A. B. Abou Hammad, Int. J. Environ. Sci. Technol. (2020).
22. M. J. Molaei, A. Ataie, S. Raygan, S. J. Picken, and F. D. Tichelaar, J. Supercond. Nov. Magn. **25**, 519 (2012).
23. K. Simeonidis, C. Martinez-Boubeta, D. Serantes, S. Ruta, O. Chubykalo-Fesenko, R. Chantrell, J. Oró-Solé, L. Balcells, A. S. Kamzin, R. A. Nazipov, A. Makridis, and M. Angelakeris, ACS Appl. Nano Mater. **3**, 4465 (2020).
24. J. Tuček, L. Machala, S. Ono, A. Namai, M. Yoshikiyo, K. Imoto, H. Tokoro, S. I. Ohkoshi, and R. Zbořil, Sci. Rep. **5**, 1 (2015).
25. Y. Chen, Y. Liu, Y. Shi, J. Ping, J. Wu, and H. Chen, TrAC - Trends Anal. Chem. **127**, (2020).
26. A. M. El Nahrawy, B. A. Hemdan, A. B. Abou Hammad, A. L. K. Abia, and A. M. Bakr, Silicon (2020).
27. H. Arami, A. Khandhar, D. Liggitt, and K. M. Krishnan, Chem. Soc. Rev. (2015).
28. X. L. Liu, S. Chen, H. Zhang, J. Zhou, H. M. Fan, and X. J. Liang, Adv. Mater. **31**, 1 (2019).
29. N. Z. Khatmi Maab, A. Shokuhfar, and S. Ahmadi, Int. Nano Lett. **6**, 211 (2016).
30. Y. A. B. Neolaka, Y. Lawa, J. N. Naat, A. A. P. Riwu, M. Iqbal, H. Darmokoesoemo, and H. S. Kusuma, J. Mater. Res. Technol. **9**, 6544 (2020).
31. J. Wu, D. Xiao, H. Zhao, H. He, J. Peng, C. Wang, C. Zhang, and J. He, Microchim. Acta **182**, 2299 (2015).
32. Z. Hu, X. Zhang, J. Li, and Y. Zhu, Front. Chem. **8**, 1 (2020).
33. J. Qi, Y. Chen, T. Xue, Y. Lin, S. Huang, S. Cao, X. Wang, Y. Su, and Z. Lin, Nanotechnology **31**, (2020).
34. M. L. Chen, L. M. Shen, S. Chen, H. Wang, X. W. Chen, and J. H. Wang, J. Mater. Chem. B **1**, 2582 (2013).
35. X. Wang, G. Li, and K. H. Row, J. Sep. Sci. **40**, 3301 (2017).
36. T. Miyazaki, J. Akaike, M. Kawashita, and H. N. Lim, Mater. Sci. Eng. C **99**, 68 (2019).
37. M. Sabzevari, D. Cree, and L. Wilson, **2014**, (2018).
38. P. Avouris and C. Dimitrakopoulos, Mater. Today **15**, 86 (2012).
39. K. S. Kim, Y. Zhao, H. Jang, S. Y. Lee, J. M. Kim, K. S. Kim, J. H. Ahn, P. Kim, J. Y. Choi, and B. H. Hong, Nature **457**, 706 (2009).
40. M. A. Moharram, K. M. T. Ereiba, W. El Hotaby, and A. M. Bakr, Middle East J. Appl. Sci. **05**, 23 (2015).
41. T. M. Magne, T. de Oliveira Vieira, B. Costa, L. M. R. Alencar, E. Ricci-Junior, R. Hu, J. Qu, C. Zamora-Ledezma, F. Alexis, and R. Santos-Oliveira, Colloids Surfaces B Biointerfaces **203**, (2021).
42. B. Alemour, M. H. Yaacob, H. N. Lim, and M. R. Hassan, Int. J. Nanoelectron. Mater. **11**, 371 (2018).
43. A. K. Sood, I. Lund, Y. R. Puri, H. Efstathiadis, P. Haldar, N. K. Dhar, J. Lewis, M. Dubey, E. Zakar, P. Wijewarnasuriya, D. L. Polla, and M. Fritze, Graphene - New Trends Dev. (2015).
44. J. Wang, F. Ma, W. Liang, and M. Sun, Mater. Today Phys. **2**, 6 (2017).
45. Z. Jiang, Y. Zhang, Y. W. Tan, H. L. Stormer,

and P. Kim, Solid State Commun. **143**, 14 (2007).
46. E. N. Koukaras, G. Kalosakas, C. Galiotis, and K. Papagelis, Sci. Rep. **5**, (2015).
47. S. Zhang, G. Wright, and Y. Yang, Biosens. Bioelectron. **15**, 273 (2000).
48. M. F. Craciun, S. Russo, M. Yamamoto, and S. Tarucha, Nano Today **6**, 42 (2011).
49. N. C. Homem, N. de Camargo Lima Beluci, S. Amorim, R. Reis, A. M. S. Vieira, M. F. Vieira, R. Bergamasco, and M. T. P. Amorim, Appl. Surf. Sci. **486**, 499 (2019).
50. K. A. Mahmoud, B. Mansoor, A. Mansour, and M. Khraisheh, Desalination **356**, 208 (2015).
51. Y. Li, X. Wu, Z. Li, S. Zhong, W. Wang, A. Wang, and J. Chen, Talanta **144**, 1279 (2015).
52. R. Mas-Ballesté, C. Gómez-Navarro, J. Gómez-Herrero, and F. Zamora, Nanoscale **3**, 20 (2011).
53. A. M. El Nahrawy, A. B. Abou Hammad, A. M. bakr, T. I. Shaheen, and A. M. Mansour, Appl. Phys. A Mater. Sci. Process. **126**, 1 (2020).
54. A. A. Al-esnawy, K. T. Ereiba, A. M. Bakr, and A. S. Abdraboh, J. Mol. Struct. (2021).
55. W. El hotaby, A. M. Bakr, H. S. Ibrahim, N. S. Ammar, H. A. Hani, and A. A. Mostafa, J. Mol. Struct. **1241**, 130605 (2021).
56. P. Dramou, A. Itatahine, M. Fizir, Y. Ait Mehdi, P. T. Kutoka, and H. He, J. Chromatogr. B Anal. Technol. Biomed. Life Sci. **1124**, 273 (2019).
57. P. Dramou, S. L. Dahn, F. Wang, Y. Sun, Z. Song, H. Liu, and H. He, TrAC - Trends Anal. Chem. **137**, 116211 (2021).
58. P. Fang, W. Xia, Y. Zhou, Z. Ai, W. Yin, M. Xia, J. Yu, R. A. Chi, and Q. Yue, Chem. Eng. J. **385**, 123847 (2020).
59. X. Luo, C. L. Weaver, S. Tan, and X. T. Cui, J. Mater. Chem. B **1**, 1340 (2013).
60. S. Goenka, V. Sant, and S. Sant, J. Control. Release **173**, 75 (2014).
61. L. P. Lingamdinne, Y. L. Choi, I. S. Kim, J. K. Yang, J. R. Koduru, and Y. Y. Chang, J. Hazard. Mater. **326**, 145 (2017).
62. X. Zhang, Q. H. Tan, J. Bin Wu, W. Shi, and P. H. Tan, Nanoscale **8**, 6435 (2016).
63. J. Y. Lim, N. M. Mubarak, E. C. Abdullah, S. Nizamuddin, M. Khalid, and Inamuddin, J. Ind. Eng. Chem. **66**, 29 (2018).
64. M. Taghioskoui, Mater. Today **12**, 34 (2009).
65. M. S. A. Bhuyan, M. N. Uddin, M. M. Islam, F. A. Bipasha, and S. S. Hossain, Int. Nano Lett. **6**, 65 (2016).
66. R. Ciriminna, N. Zhang, M. Q. Yang, F. Meneguzzo, Y. J. Xu, and M. Pagliaro, Chem. Commun. **51**, 7090 (2015).
67. A. M. ElNahrawy and A. B. AbouHammad, Int. J. PharmTech Res. **9**, 16 (2016).
68. M. Kamal, I. K. Battisha, M. A. Salem, and A. M. S. El Nahrawy, J. Sol-Gel Sci. Technol. **58**, 507 (2011).
69. A. B. Abou Hammad, A. M. Elnahrawy, A. M. Youssef, and A. M. Youssef, Int. J. Biol. Macromol. **125**, 503 (2019).
70. J. Phiri, P. Gane, and T. C. Maloney, Mater. Sci. Eng. B Solid-State Mater. Adv. Technol. **215**, 9 (2017).
71. K. S. Novoselov, V. I. Fal'Ko, L. Colombo, P. R. Gellert, M. G. Schwab, and K. Kim, Nature **490**, 192 (2012).
72. Y. Wu, B. Wang, Y. Ma, Y. Huang, N. Li, F. Zhang, and Y. Chen, Nano Res. **3**, 661 (2010).
73. Y. Hernandez, V. Nicolosi, M. Lotya, F. M. Blighe, Z. Sun, S. De, I. T. McGovern, B. Holland, M. Byrne, Y. K. Gun'ko, J. J. Boland, P. Niraj, G. Duesberg, S. Krishnamurthy, R. Goodhue, J. Hutchison, V. Scardaci, A. C. Ferrari, and J. N. Coleman, Nat. Nanotechnol. **3**, 563 (2008).
74. Y. Xu, H. Cao, Y. Xue, B. Li, and W. Cai, Nanomaterials **8**, (2018).
75. W. Luheng, D. Tianhuai, and W. Peng, Carbon N. Y. **47**, 3151 (2009).
76. K. Parvez, R. Li, S. R. Puniredd, Y. Hernandez, F. Hinkel, S. Wang, X. Feng, and K. Müllen, ACS Nano **7**, 3598 (2013).
77. S. Barcikowski, F. Devesa, and K. Moldenhauer, J. Nanoparticle Res. **11**, 1883 (2009).
78. E. Cappelli, S. Orlando, M. Servidori, and C. Scilletta, Appl. Surf. Sci. **254**, 1273 (2007).
79. K. A. Madurani, S. Suprapto, N. I. Machrita, S. L. Bahar, W. Illiya, and F. Kurniawan, ECS J. Solid State Sci. Technol. **9**, 093013 (2020).
80. S. S. Shams, L. S. Zhang, R. Hu, R. Zhang, and J. Zhu, Mater. Lett. **161**, 476 (2015).
81. Z. Y. Juang, C. Y. Wu, C. W. Lo, W. Y. Chen, C. F. Huang, J. C. Hwang, F. R. Chen, K. C. Leou, and C. H. Tsai, Carbon N. Y. **47**, 2026 (2009).
82. Y. Pan, H. Zhang, D. Shi, J. Sun, S. Du, F. Liu, and H. J. Gao, Adv. Mater. **21**, 2777 (2009).
83. D. A. C. Brownson and C. E. Banks, Phys. Chem. Chem. Phys. **13**, 15825 (2011).
84. F. Yavari, Z. Chen, A. V. Thomas, W. Ren, H. M. Cheng, and N. Koratkar, Sci. Rep. **1**, 1 (2011).
85. V. B. Mbayachi, E. Ndayiragije, T. Sammani, S. Taj, E. R. Mbuta, and A. ullah khan, Results Chem. **3**, 100163 (2021).
86. S. Kim, Y. Song, J. Wright, and M. J. Heller, Carbon N. Y. **102**, 339 (2016).
87. E. F. D. Januário, T. B. Vidovix, N. de C. L. Beluci, R. M. Paixão, L. H. B. R. da Silva, N. C. Homem, R. Bergamasco, and A. M. S. Vieira, Sci. Total Environ. **789**, (2021).
88. H. Yu, B. Zhang, C. Bulin, R. Li, and R. Xing, Sci. Rep. **6**, 1 (2016).
89. H. Mehl, C. F. Matos, E. G. C. Neiva, S. H. Domingues, and A. J. G. Zarbin, Quim. Nova **37**, 1639 (2014).
90. Y. He, C. Yi, X. Zhang, W. Zhao, and D. Yu,

TrAC - Trends Anal. Chem. **136**, (2021).
91. J. Hur, J. Shin, J. Yoo, and Y. S. Seo, Sci. World J. **2015**, (2015).
92. A. B. Abou Hammad, A. G. Darwish, and A. M. El Nahrawy, Appl. Phys. A Mater. Sci. Process. **126**, 1 (2020).
93. A. M. Mansour, A. B. Abou Hammad, and A. M. El Nahrawy, Nano-Structures and Nano-Objects **25**, 100646 (2021).
94. H. Iida, K. Takayanagi, T. Nakanishi, and T. Osaka, J. Colloid Interface Sci. **314**, 274 (2007).
95. R. Hong, J. Li, J. Wang, and H. Li, China Particuology **5**, 186 (2007).
96. C. K. Chua and M. Pumera, Chem. Soc. Rev. **43**, 291 (2014).
97. Q. Zhou, Y. Wang, J. Xiao, and H. Fan, Sci. Rep. **7**, 1 (2017).
98. S. F. O. Microparticles, Organ, The (n.d.).
99. A. M. El Nahrawy, B. A. Hemdan, A. B. Abou Hammad, A. M. Othman, A. M. Abouelnaga, and A. M. Mansour, Silicon **13**, 2979 (2021).
100. J. Zhou, H. Song, L. Ma, and X. Chen, RSC Adv. **1**, 782 (2011).
101. M. J. Molaei, Mater. Sci. Eng. B Solid-State Mater. Adv. Technol. **272**, 115325 (2021).
102. Y. B. Luo, Z. G. Shi, Q. Gao, and Y. Q. Feng, J. Chromatogr. A **1218**, 1353 (2011).
103. S. Pei, Q. Wei, K. Huang, H. M. Cheng, and W. Ren, Nat. Commun. **9**, 1 (2018).
104. W. Zhang, G. Yang, X. Wang, L. Jiang, F. Jiang, G. Li, Z. Zhang, and X. Jiang, Adv. Mater. **29**, 1 (2017).
105. G. Huang, X. Zhu, H. Li, L. Wang, X. Chi, J. Chen, X. Wang, Z. Chen, and J. Gao, Nanoscale **7**, 2667 (2015).
106. Y. Luo, Y. Tang, T. Liu, Q. Chen, X. Zhou, N. Wang, M. Ma, Y. Cheng, and H. Chen, Chem. Commun. **55**, 1963 (2019).
107. A. Jafarizad, A. Taghizadehgh-Alehjougi, M. Eskandani, M. Hatamzadeh, M. Abbasian, R. Mohammad-Rezaei, M. Mohammadzadeh, B. Toğar, and M. Jaymand, Biomed. Mater. Eng. **29**, 177 (2018).
108. X. Ma, H. Tao, K. Yang, L. Feng, L. Cheng, X. Shi, Y. Li, L. Guo, and Z. Liu, Nano Res. **5**, 199 (2012).
109. Y. J. Lu, P. Y. Lin, P. H. Huang, C. Y. Kuo, K. T. Shalumon, M. Y. Chen, and J. P. Chen, Nanomaterials **8**, 1 (2018).
110. C. Liang, J. Song, Y. Zhang, Y. Guo, M. Deng, W. Gao, and J. Zhang, Nanoscale Res. Lett. **15**, 1 (2020).
111. R. O. Rodrigues, G. Baldi, S. Doumett, L. Garcia-Hevia, J. Gallo, M. Bañobre-López, G. Dražić, R. C. Calhelha, I. C. F. R. Ferreira, R. Lima, H. T. Gomes, and A. M. T. Silva, Mater. Sci. Eng. C **93**, 206 (2018).
112. Y. Li, T. Jing, G. Xu, J. Tian, M. Dong, Q. Shao, B. Wang, Z. Wang, Y. Zheng, C. Yang, and Z. Guo, Polymer (Guildf). **149**, 13 (2018).
113. Q. U. Ain, M. U. Farooq, and M. I. Jalees, J. Water Process Eng. **33**, 101044 (2020).
114. B. Yang, Y. Wei, Q. Liu, Y. Luo, S. Qiu, and Z. Shi, Colloids Surfaces A Physicochem. Eng. Asp. **582**, 123927 (2019).
115. Y. Lei, F. Chen, Y. Luo, and L. Zhang, J. Mater. Sci. **49**, 4236 (2014).
116. G. Abdi, A. Alizadeh, J. Amirian, S. Rezaei, and G. Sharma, J. Mol. Liq. **289**, 111118 (2019).
117. T. T. N. Le, V. T. Le, M. U. Dao, Q. V. Nguyen, T. T. Vu, M. H. Nguyen, D. L. Tran, and H. S. Le, Chem. Eng. Commun. **206**, 1337 (2019).
118. Z. Dai, Y. Sun, H. Zhang, D. Ding, and L. Li, Ind. Eng. Chem. Res. **58**, 19280 (2019).
119. H. R. Nodeh, M. A. Kamboh, W. A. Wan Ibrahim, B. H. Jume, H. Sereshti, and M. M. Sanagi, Environ. Sci. Process. Impacts **21**, 714 (2019).
120. H. Fakhri, M. Farzadkia, R. Boukherroub, V. Srivastava, and M. Sillanpää, Sol. Energy **208**, 990 (2020).